IOP Publishing Biomed. Mater. 17 (2022) 055015 https://doi.org/10.1088/1748-605X/ac885a

Biomedical Materials

OPEN ACCESS

RECEIVED
9 November 2021

REVISED
20 July 2022

ACCEPTED FOR PUBLICATION
8 August 2022

PUBLISHED
23 August 2022

PAPER

Hybrid fibroin/polyurethane small-diameter vascular grafts: from fabrication to *in vivo* preliminary assessment

Alice Caldiroli[1,6], Elia Pederzani[2,6], Marco Pezzotta[2], Nadia Azzollini[3], Sonia Fiori[3], Matteo Tironi[3], Paola Rizzo[3], Fabio Sangalli[3], Marina Figliuzzi[3], Gianfranco Beniamino Fiore[2], Andrea Remuzzi[4], Stefania Adele Riboldi[5], Monica Soncini[2,*] and Alberto Redaelli[2]

[1] Bioengineering Laboratories Srl, Via Vivaldi 32/A, Cantù, 22063, Italy
[2] Politecnico di Milano Dipartimento di Elettronica Informazione e Bioingegneria, Via Giuseppe Ponzio 34, Milano, 20133, Italy
[3] Istituto di Ricerche Farmacologiche Mario Negri IRCCS, Via Stezzano 87, Bergamo, 24126, Italy
[4] Università degli Studi di Bergamo, Via Pignolo 123, Bergamo, Lombardia, 24121, Italy
[5] Dialybrid S.r.l., R&D, Via Vivaldi 32/A, Cantù, 22063, Italy
[6] These authors contributed equally.
[*] Author to whom any correspondence should be addressed.

E-mail: monica.soncini@polimi.it

Keywords: hybrid vascular graft, silk fibroin, radial compliance, rodent model

Supplementary material for this article is available online

Abstract

To address the need of alternatives to autologous vessels for small-calibre vascular applications (e.g. cardiac surgery), a bio-hybrid semi-degradable material composed of silk fibroin (SF) and polyurethane (Silkothane®) was herein used to fabricate very small-calibre grafts ($Ø_{in} = 1.5$ mm) via electrospinning. Bio-hybrid grafts were *in vitro* characterized in terms of morphology and mechanical behaviour, and compared to similar grafts of pure SF. Similarly, two native vessels from a rodent model (abdominal aorta and vena cava) were harvested and characterized. Preliminary implants were performed on Lewis rats to confirm the suitability of Silkothane® grafts for small-calibre applications, specifically as aortic insertion and femoral shunt. The manufacturing process generated pliable grafts consisting of a randomized fibrous mesh and exhibiting similar geometrical features to rat aortas. Both Silkothane® and pure SF grafts showed radial compliances in the range from 1.37 ± 0.86 to $1.88 \pm 1.01\%$ 10^{-2} $mmHg^{-1}$, lower than that of native vessels. The Silkothane® small-calibre devices were also implanted in rats demonstrating to be adequate for vascular applications; all the treated rats survived the surgery for three months after implantation, and 16 rats out of 17 (94%) still showed blood flow inside the graft at sacrifice. The obtained results lay the basis for a deeper investigation of the interaction between the Silkothane® graft and the implant site, which may deal with further analysis on the potentialities in terms of degradability and tissue formation, on longer time-points.

1. Introduction

Cardiovascular diseases are acknowledged to be one of the leading causes of death around the world (∼31%), lethally affecting 17.9 million people during 2019 [1]. Vascular surgery is often necessary to treat diseases of the circulatory system and other pathologies, as it happens for end-stage renal disease, which requires a vascular access to perform haemodialysis therapy. Autologous solutions are still the first choice, as they are not subject to biocompatibility issues: typically, coronary artery bypass grafting is performed involving the saphenous vein or the internal mammary artery [2] and an arteriovenous fistula is created as vascular access for haemodialysis [3]. Unfortunately, autologous vessels are not always available, may not be sufficient for multiple bypass or may be affected by degenerative alterations that impede the repetitive punctures fundamental in case of haemodialysis [4]; from this perspective, the urgent need of alternatives is clear. Traditional synthetic materials, e.g. polyethylene terephthalate (PET) and

expanded polytetrafluoroethylene (ePTFE), which can successfully replace large vessels (Ø > 6 mm) [5–7], are not adequate in case of small (Ø < 6 mm) and very small (Ø ∼ 1.5 mm) calibre vessels because of their low patency rate [8], as they are prone to aneurysm formation, neo-intimal hyperplasia, calcification, thrombosis and infections [4, 9, 10]. This may be imputable to the formation of a non-functional endothelium [9] elicited by the difference in mechanical properties, i.e. radial compliance [11], between grafts and native vessels.

Tissue engineering (TE) aims to overcome these limitations, developing a vascular construct which is biologically and mechanically close to native vessels [12]; specifically, *in situ* TE relies on the implantation of degradable or semi-degradable scaffolds as they are in the destination site [13]. Due to their specific structure and composition, they are able to guide and control cell recruitment, differentiation, and tissue formation at the site of implantation [14, 15], turning into functional endogenous living tissues [10]. Before tissue formation, the scaffold must sustain the hemodynamic stimuli alone, being mechanically robust, and its degradation rate should balance the generation of new biological tissue to avoid implant's failure [16–18]. Xeltis B.V. (Eindhoven, Netherlands) developed a flexible and highly porous conduit (Ø = 18–20 mm), composed of a bio-resorbable polyester, designed to trigger a series of physiological events that lead to endogenous tissue restoration. This device, intended for by-pass grafting or as vascular access, has been implanted as total cavopulmonary connection in paediatric patients in a pioneering clinical trial [19, 20]. Another approach consists in blending different materials, natural and/or synthetic, in order to maximize scaffold's properties and characteristics [21–26], and, in particular, the combination of silk fibroin (SF), a biodegradable and highly biocompatible protein, and polyurethanes (PUs), was proved to be promising hybrid solution in TE [27–30].

Basing on these assumptions, van Uden *et al* [31] developed Silkothane® blending SF with an aromatic and bioinert PU, to combine the bioactivity of SF with the elasticity of PU. Conventional Fourier transform infrared spectroscopy and differential scanning calorimetry confirmed that the features of both SF and PU are retained within Silkothane®. Processing it via electrospinning, it was possible to obtain a porous scaffold that well mimics the extracellular matrix and favours cells proliferation [32–34]. A three-layered conduit ($Ø_{in}$ = 6–8 mm), where Silkothane® is enclosed within two layers of pure SF, was designed to enhance graft biocompatibility [35]. Silkothane® grafts proved to guarantee a non-haemolytic character, a long clotting time and a significant adhesion of human umbilical vein endothelial cells with increasing viability up to seven days, superior to commercial grafts composed of electrospun PU and ePTFE. Later, an *in vivo* proof-of-concept study was performed on ovine model where Silkothane® grafts were implanted as arteriovenous shunts [36].

The present study aims to scale the previous medium-calibre Silkothane® grafts [31, 35, 36], down to the very small-calibre ($Ø_{in}$ = 1.5 mm), as regards feasibility of manufacturing and grafts' mechanical behaviour. Matter of investigation is the possible enhancement of the graft's radial compliance that follows the introduction of a high percentage of PU (75% w/w) in the Silkothane® core of the graft itself [35]. Three-layered (3L) Silkothane® grafts and a control group of one layer of pure SF (1L SF), were manufactured and extensively characterized with the aim of highlighting possible differences related to the Silkothane® core. Moreover, to confirm the *in vivo* potentiality of 3L Silkothane® grafts for small-calibre application, they were implanted in a rodent model (Lewis rats) in arterial and arteriovenous configuration according to previous work (see [37] and [36], respectively). Evaluations were made considering graft surgical usability, patency and tissue remodelling after three months. To correctly estimate the properties of the native arterial and venous tissue of the specific animal model, a mechanical characterization of the rat abdominal aorta (AA) and vena cava (VC) was also performed.

2. Materials and methods

2.1. Vascular grafts manufacturing

Three-layered grafts (3L Silkothane®, figure 1(a)), composed of a nanometric mesh of SF and PU enclosed within SF layers, were manufactured, as well as monolayers of pure SF (1L SF, figure 1(b)), which represent the control group. In the following, fabrication techniques and protocols are described.

2.1.1. Materials

Silk *Bombyx mori* cocoons were provided by the Council of Research and Experiments in Agriculture, Apiculture and Sericulture Unit (CREA-API; Padua, Italy) and regenerated SF was obtained as previously described [31]. Briefly, sericin was removed by degumming and fibroin fibres were dissolved in lithium bromide solution, diluted with warm deionized water, filtered and dialysed; regenerated SF films were obtained by solvent casting. Poly-carbonate-urethane (Carbothane™ Aromatic, AC-4075A) pellets were provided by Lubrizol (Wickliffe, OH, United States), while formic acid (FA) and dichloromethane (DCM) by Carlo Erba Reagents (Cornaredo, Italy).

2.1.2. Preparation of electrospinning solutions

Fibroin solution was prepared by cutting SF films into ∼2 × 2 mm pieces and dissolving them in FA at 2.5% or 7% (w/v) concentration, stirring for 1 h at 155 rpm. PU solution was prepared by dissolving the pellets at 5% (w/v) in a blend of FA and DCM with 1:2 volume ratio, stirring for 1 h at 250 rpm. Silkothane® solution

Table 1. Electrospinning parameters for both 3L Silkothane® and 1L SF vascular grafts. SF: silk fibroin, PU: polyurethane, FA: formic acid, DCM: dichloromethane, t: electrospinning time, ΔV: applied voltage, Q: solution flow rate, ω rotational speed of the collector, d: distance between the tip of the spinneret and the collector.

	%SF (w/v)	%PU (w/v)	FA:DCM (v:v)	t (hh:mm)	ΔV (kV)	Q (ml h^{-1})	ω (rpm)	d (mm)
 3L Silkothane®	7	0	1:0	00:10	24	1.5	2500	120
	1	3	3:2	00:45	21	2.5	1000	120
	7	0	1:0	00:10	24	1.5	2500	120
 1L SF	7	0	1:0	00:25	24	1.5	2500	120

was obtained by mixing the 2.5% fibroin solution and the PU solution for 15 min at 155 rpm, resulting in a 4% (w/v) concentration solution of SF and PU (1:3) in FA and DCM (3:2).

2.1.3. Electrospinning process

Both 3L Silkothane® and 1L SF grafts were manufactured electrospinning the prepared solutions, setting process parameters as described in table 1, and following the typical protocol described in [35]. Briefly, a syringe pump, equipped with a solvent-resistant syringe (10 ml, Norm-Ject luer slip, VWR), delivered a controlled flow rate of solution to the horizontally translating spinneret (18 G, velocity = 5 mm s^{-1}, stroke = 200 mm). Fibres generated at the tip of the spinneret due to the difference in voltage between the spinneret (positively charged) and the cylindrical stainless steel rotating collector (grounded, Ø = 1.5 mm). To facilitate grafts removal, the collector was previously dipped into a saturated solution of demineralized water and soap and left to dry ∼2 h before the electrospinning session.

2.1.4. Post-fabrication treatment

At the end of the electrospinning process, the tubular grafts were removed from the collector, washed and crystallized as previously described [31] (figures 1(c) and (d)). Briefly, they were immersed into five descending series of ethanol/demineralized water solutions (1:1 for 1 h, 1:1 for ∼18 h, 1:3 for 1 h, 1:3 for 1 h and 0:1 for 1 h) and left to dry overnight. Then, samples were vacuum dried (∼2.5 kPa, RT) for about 4 h and sterilized with ethylene oxide at STERIS S.p.A. (Calcinate, Italy).

2.2. Native vessels harvesting

Lewis rats (n = 10) were purchased from Charles River Laboratories (Calco—Lc, Italy) and were maintained in the animal care facility of 'Istituto di Ricerche Farmacologiche Mario Negri IRCCS' with a 12 h dark and 12 h light cycle, in a constant temperature room and with free access to standard diet and water. Rats were euthanized by CO_2 inhalation, and AA and VC were collected for mechanical tests. Briefly, after exposing the abdominal cavity, the artery was detached from the vein and the collaterals of both vessels were closed with the suture threads sutures. About 2 cm of vein and artery were removed and placed in Servator B buffer (S.A.L.F.—Cenate Sotto, BG). For each sample, the distance between two marked reference points was measured pre- (figures 1(e) and (f)) and post-explant (figures 1(g) and (h)), to collect data about *in vivo* vessel tensioning to be reproduced during *in vitro* compliance measurements. Three VCs out of ten were excluded from the study as the explant procedure damaged their walls making them unsuitable for mechanical characterization.

2.3. Morphological and dimensional analysis

Grafts thickness (th, mm) and diameter (D, mm) were measured on a thin ring of material acquiring an image by means of a camera (MU500 CK 5MP AmScope, USA) interfaced with a stereo microscope (Nikon SMZ1000) and processing it via *ImageJ* software (n_{3L} = 11 and n_{1L} = 12). Specifically, internal and external radii were derived from the corresponding cross-sectional areas of the samples assuming a circular shape, and thickness was obtained from their subtraction. Grafts mass and length were also registered using a precision balance (Crystal 200 SMI, Gibertini) and a ruler and used, together with the thickness, to derive material density (ρ, g cm^{-3}). Length was measured both in dry and wet conditions (n_{3L} = 4 and n_{1L} = 6), specifically after 10 min of hydration in demineralized water, to derive material dimensional variations (%).

SEM analysis was performed on 3L Silkothane (n = 3) and 1L SF (n = 3) samples by means of a Supra55 microscope (Zeiss, Germany) using secondary electrons detection with an acceleration voltage set to 1–4.5 kV, to observe cross sections (figures 1(i) and (j)) and fibres morphology (figures 2(a)–(d)). Fibres average diameter and orientation were measured on both the inner and the outer layers, using *ImageJ* software to analyse at least 100 fibres sections per image.

Native vessels thickness (n_{AA} = 3 and n_{VC} = 3) was measured on histological images of the sections of both AA and VC (figures 1(k) and (l)). After the explant, vessels were fixed in paraformaldehyde 4% (Electron Microscopy Sciences, Hatfield, PA, USA) overnight and embedded in optimal-cutting temperature compound. Micrometrical sections were

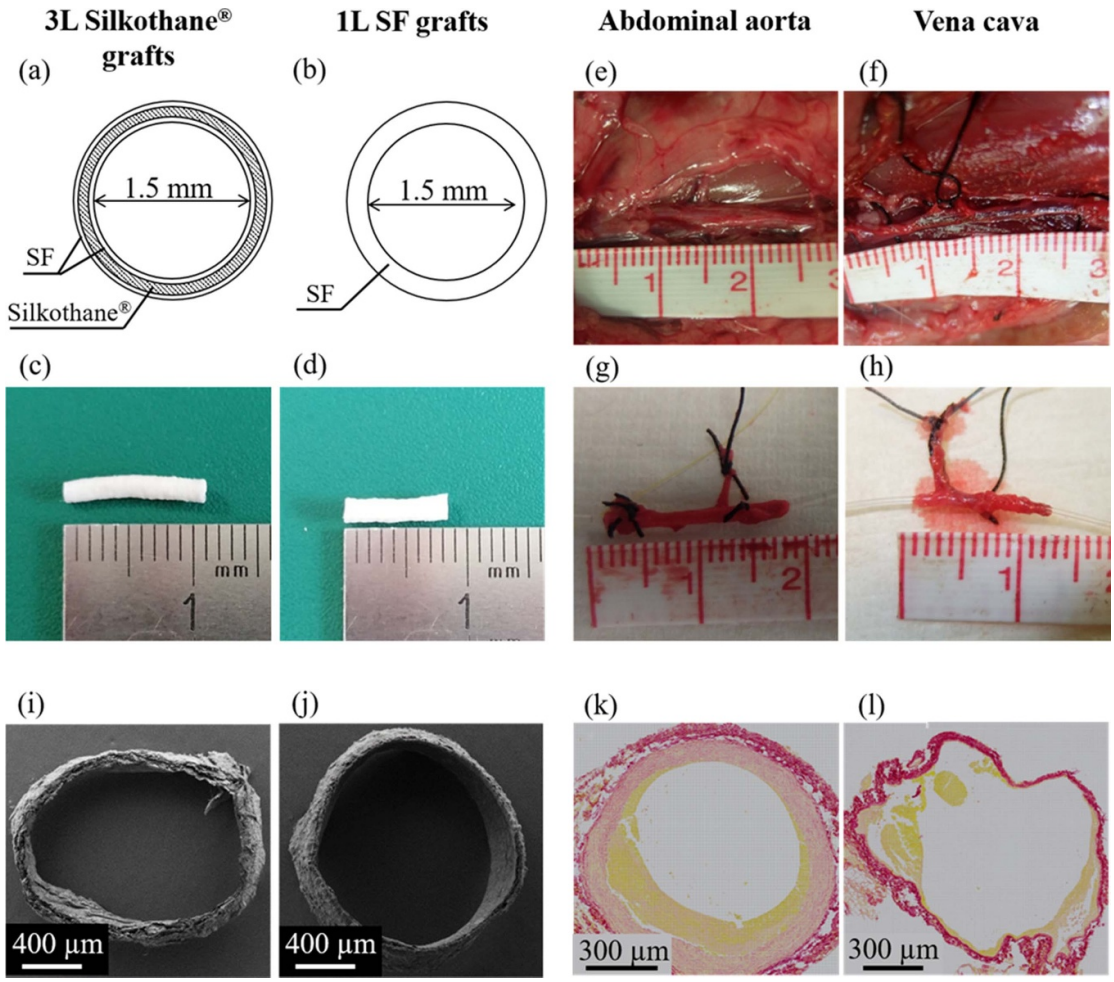

Figure 1. Schematic representation of sections of three-layered Silkothane® graft (3L Silkothane®) (a) and mono-layered pure-silk fibroin graft (1L SF) (b); macroscopic aspect of 3L Silkothane® (c) and 1L SF graft (d); rat's abdominal aorta (e) and vena cava (f) measured *in vivo*; explanted rat's abdominal aorta (g) and vena cava (h); representative sections of 3L Silkothane® (i) and 1L SF (j) graft observed via SEM; histology of representative rat's abdominal aorta (k) and vena cava (l) section stained with picrosirius red.

stained with picrosirius red and digitalized by means of a 20× magnification objective with mosaics module (Axio Observer, Zeiss). By means of *ImageJ* software, appropriate grids were applied to the images and thickness was calculated from the harmonic mean of more than 200 orthogonal lengths. To compensate for the processing-induced tissue shrinkage, measured thicknesses were increased by 25% in accordance with literature data [38, 39]. A comparison with thickness measurements on images of fresh rings of rat arteries ($n = 10$), acquired by stereomicroscope as described for grafts, was performed, confirming a difference of 25%.

2.4. Mechanical and physical characterization

2.4.1. Materials

In order to perform quasi steady compliance measurements, we used a compact device ad hoc designed for housing both grafts and native vessels (figure 3(a)). The system is able to apply a controlled intraluminal pressure to a vascular sample (component 1) hosted in a transparent reservoir filled with thermostated medium (component 2, figure 3(b)), and pretensioned by means of a screw-based system. Sample pressurization, measured by a pressure transducer (ZSE30A-C6L-P, SMC, Japan, component 5), is applied by a centrifugal pump (M400-S180, RS Pro, component 3), while the extraluminal medium recirculation is performed by a miniaturized roller pump dampened by an air chamber in order to generate a quasi-steady flow rate (component 4 and 6). A heat exchanger, consisting of a copper coil immersed in a thermostatic reservoir, is used to heat and maintain the medium at physiological temperature, (component 7).

A quasi-steady compliance measurement setup was chosen and used for this study similarly to most of the systems in literature [21, 40, 41], as it allows to perform experiments under repeatable conditions enabling temperature control, imposed pressure accuracy, and image acquisition. Experiments were carried out at 37 ± 2 °C with Servator B buffer (S.A.L.F.—Cenate Sotto, BG, Italy) as intraluminal and extraluminal fluid. A stereo

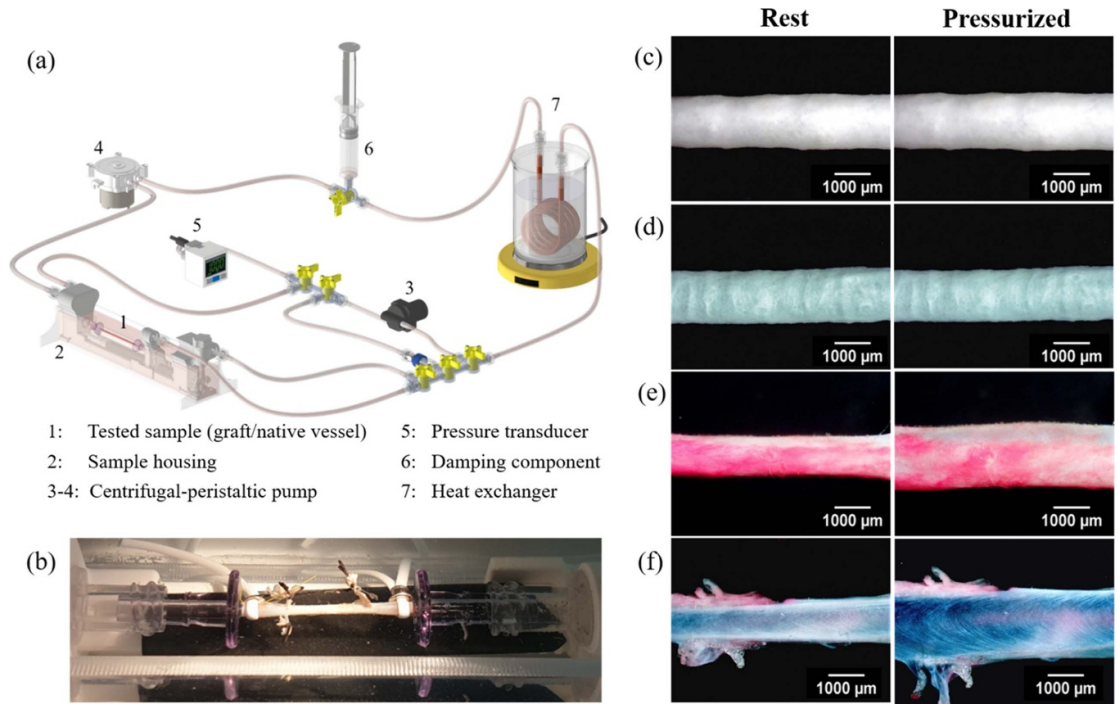

Figure 2. (a) Experimental setup employed in radial compliance, viscoelasticity and water permeability measurements; (b) example of a native vessel assembled in the sample housing; (c) 3L Silkothane® graft at rest (0 mmHg) and pressurized (150 mmHg); (d) 1L SF graft at rest and pressurized (150 mmHg); (e) rat's AA at rest and pressurized (150 mmHg); (f) rat's VC at rest and pressurized (40 mmHg).

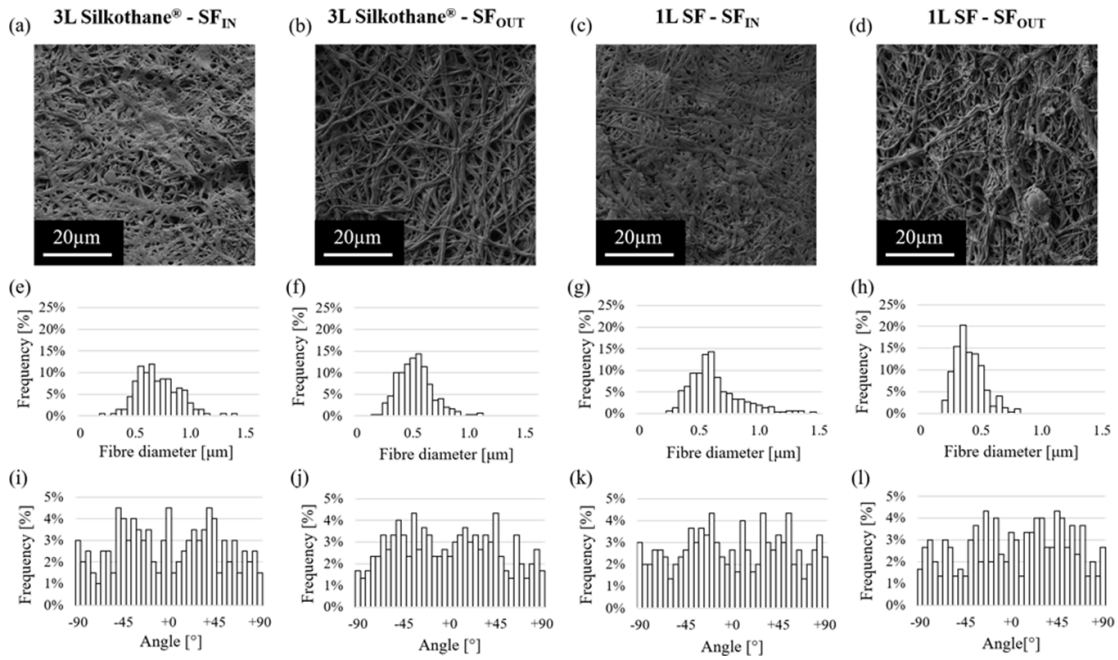

Figure 3. Morphological analysis of silk fibroin fibres: high magnification SEM images of the inner and the outer layers of 3L Silkothane® (a), (b) and 1L SF (c), (d) grafts; frequency distributions of fibres diameters (e)–(h) and angles (i)–(l).

microscope (Nikon SMZ1000) equipped with a digital camera (MU500 CK 5MP, AmScope, USA) was used for image acquisition. Radial compliance (C, % 10^{-2} mmHg^{-1}) of grafts ($n_{3L} = 11$ and $n_{1L} = 12$) and native vessels ($n_{AA} = 10$ and $n_{VC} = 7$) was measured by pressurizing them and acquiring the corresponding dimensional variations, according to equation (1) in standard ISO 7198:2016 on the characterization of vascular grafts [42]

$$C = \frac{\left(D_{P_{max}} - D_{P_{min}}\right)/D_{P_{min}}}{P_{max} - P_{min}} \times 10^4 \qquad (1)$$

where P_{max} and P_{min} (mmHg) are the extremes of the pressure range of interest and D_{Pmax} and D_{Pmin} (mm) are the related internal diameters. During the experiments native vessels were tensioned by reproducing the *in vivo* vessel tension measured as reported in section 2.2. Radial compliance of grafts and AAs was measured in the following ranges: 50–90, 80–120, and 110–150 mmHg, which mimic hypo-, normo-, and hypertension conditions, respectively. Starting from the resting condition (0 mmHg), intraluminal pressure was increased up to 150 mmHg with steps of 10 mmHg. Ranges considered in case of VC were 10–20, 20–30, and 30–40 mmHg, as the *in vivo* pressure rarely exceeds such values [43]; in the case of VC, 2–3 mmHg increments were performed. The selected pressure ranges are reasonable with both the physiological conditions [43] and the arteriovenous shunt ones which, as reported in literature [44], result in a decreased mean arterial pressure (108 ± 2 vs 89 ± 1 mmHg) and an increased venous pressure (4.5 ± 1.6 vs 16.4 ± 3.9 mmHg). At each pressure step, a digital image was acquired by means of the camera, so that the progressive increase of sample's external diameter was recorded (figures 3(c)–(f)). These images were analysed by means of *ImageJ* software to derive the averaged external diameters at any pressure point. After a manual removal of the macroscopic defects, images were binarized setting the proper threshold for each one considering its specific histogram. A set of 50 equally spaced parallel lines of background colour was superimposed to a duplicate of the binarized image and positioned perpendicularly to the graft/vessel longitudinal axis. Subtracting the elaborated image to the other allowed the extraction of 50 measurements of sample external diameter. The mean value was calculated excluding measures that differ from the average more than 5%. Internal diameters were derived by subtracting twice the thickness, as measured in section 2.3, from the averaged external diameters.

For sake of comparison with literature data, diameter distensibility (D_d) was also estimated for AA rat arteries in the 0–100 mmHg pressure range and was calculated as reported in equation (2):

$$D_d = 2\frac{(D_{P_{max}} - D_{P_{min}})/D_{P_{min}}}{P_{max} - P_{min}} \quad (2)$$

where P_{max} and P_{min} are equal to 100 and 0 mmHg, respectively.

2.4.2. Viscoelasticity

The viscoelastic properties of 3L Silkothane® grafts ($n_{3L} = 3$, $n_{1L} = 3$) were tested under cyclic stimulation in order to adhere to *in vivo* conditions. The setup used for radial compliance measurements (figure 3(a)) was herein employed to pressurize the samples from 0 to 150 mmHg and back, acquiring images at each 10 mmHg pressure step that were then analysed via ImageJ software to derive the diameter, as described in section 2.4.1. Viscoelasticity was investigated observing the increasing of the diameter at 100 mmHg between the first and the last cycle (D_1 vs D_{15}, equation (3)) and the variation of the hysteresis curves

$$\frac{D_{15} - D_1}{D_1} \times 100. \quad (3)$$

2.4.3. Water permeability

Water permeability of grafts ($n_{3L} = 10$, $n_{1L} = 11$) was measured in accordance with ISO 7198:2016 (section A.5.1.3) [42]. Before testing, samples were hydrated in demineralized water for at least 10 min. The same set up used for compliance measurements (figure 3(a)) was employed to pressurize tested samples with demineralized water ($T = 37 \pm 2$ °C) at 120 ± 2 mmHg and to collect the leakage volume in a recorded time interval. Water flow rate (Q, ml min^{-1}) was then derived and used to calculate samples water permeability (K, ml min^{-1} cm^{-2}) by dividing Q by the lateral graft surface (A, cm^2).

2.5. Preliminary implantation tests

Silkothane® cytotoxicity and biocompatibility have been already evaluated to verify the possibility to implant three-layered grafts ($D_{in} = 6$ mm) in animals [35]. To check whether the scaling to very small calibre and related procedures do affect these properties, cell viability was assessed via resazurin assay, deriving cell metabolic activity that increased over time (cell viability % vs control from 84 ± 11.2 to 124 ± 3.5). Moreover, SEM analysis revealed the presence of a continuous cell monolayer of human umbilical vein endothelial cells (HUVECs) adhered over the luminal side of the Silkothane® graft samples after seven days (cell viability % graph and SEM image are available as supplementary material). To verify the usability of the manufactured and characterized 3L Silkothane® grafts, a preliminary animal study on rodent model was performed as proof-of-concept, involving 17 inbred Lewis rats. As the suitability of pure SF small-calibre grafts was already proved by other research groups [45, 46], we decided not to use 1L SF grafts as control. 3L Silkothane® grafts were implanted via microsurgical technique in aseptic conditions on a thermostated operating table ($T = 37$ °C), administering Carprofen to the animal via subcutaneous injection (dose of 5 mg kg^{-1}). Grafts were implanted in two different anatomic regions, namely aortic insertion ($n = 10$) and femoral shunt ($n = 7$).

The aortic insertion was realized via laparotomy, using an approximator clamp to isolate the AA from the circulatory system and performing an arteriotomy. The graft (length ∼ 5 mm) was positioned between the stumps and connected to them with eight independent sutures (thread 10/0), creating two end-to-end anastomoses; thereby, the graft resulted as substitutive of an aortic tract (figure 4(a)). In rats that

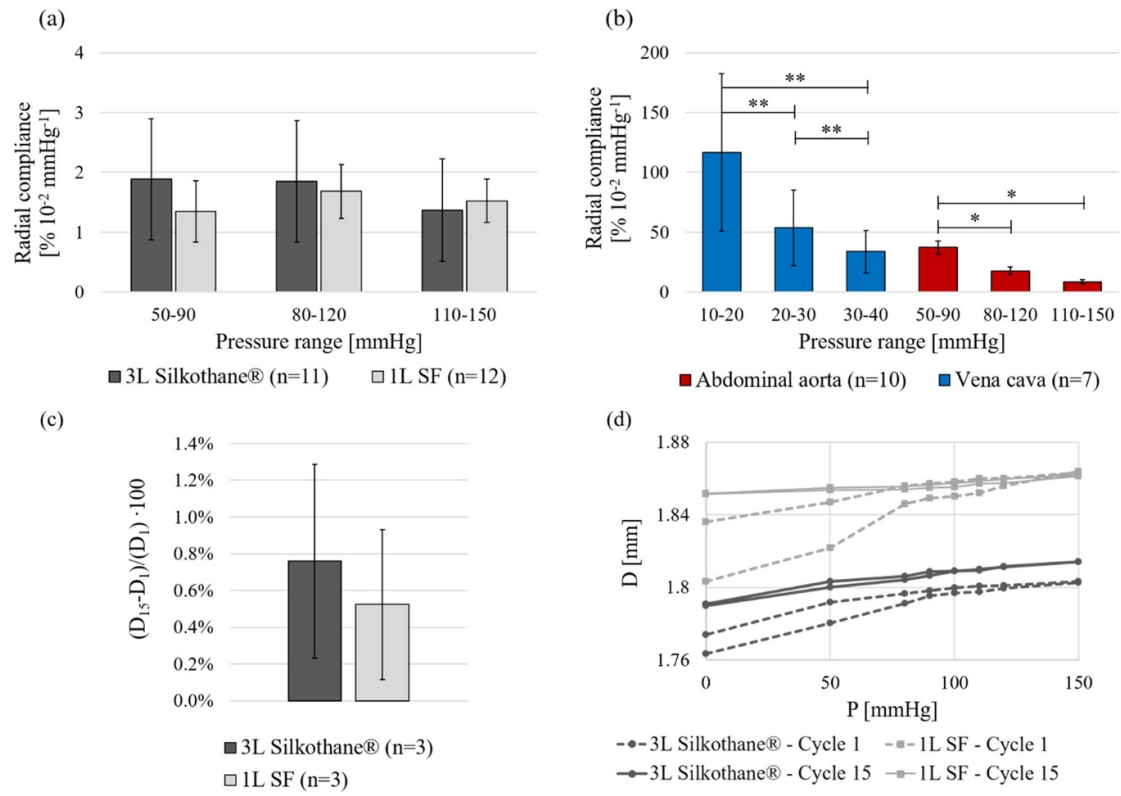

Figure 4. Radial compliance of (a) electrospun 3L Silkothane® and 1L SF grafts and (b) rat's abdominal aorta and vena cava. Viscoelastic behaviour of 3L Silkothane® and 1L SF grafts: (c) percentage variation of the diameter at 100 mmHg between the 1st and the 15th stimulation cycle; (d) comparison of the hysteresis curves of the 1st and the 15th cycle. Results are expressed as mean ± standard deviation. * $p < 0.05$; ** $p < 0.001$.

received the femoral shunt, a cutaneous incision was performed to the groin in parallel to the spine, exposing the femoral artery and the femoral vein. Again, the approximator was used to clamp the two vessels and a 2 mm cut was performed on each vessel, where continuous sutures were created to anastomose the graft (length $\sim$ 2 mm) with $a \sim 45°$ angle in two end-to-side configurations (figure 4(e)).

The vessels were then re-perfused, the incisions were sutured and the rats were kept in a thermostatic chamber ($T = 23$ °C–26 °C) where they recover from anaesthesia, avoiding hypothermia until the restoring of physiological conditions. Rats were delivered with 0.25 mg ml^{-1} ($\sim$20 ml) antibiotic therapy (Enrofloxacin) via drinking water from one day before to one week after the surgery (eight days).

Graft functionality was monitored via Echo-Doppler (Mindray M9 Ultrasound System) during the following weeks (every week during the first month and every two weeks from one month after the surgery to the explant). Signs of general discomfort and/or neurological damages related to the clinical situation were continuously checked. Rats were euthanized three months after surgery, and grafts, together with the anastomosis and part of the vessels, were explanted fixed in 4% formalin and embedded in paraffin for histological analysis. Three-micrometre-thick sections, obtained by cutting at different depths to understand the geometry of the samples, were stained with haematoxylin and eosin and digitized using a 10× magnification objective with mosaics module (Axio Observer, Zeiss). Paraffin-embedded sections were then deparaffinized and hydrated for immunofluorescence staining. Antigen retrieval was performed using a Decloaking chamber (DC NxGen 220 V, Biocare Medical) for 15 min at 110 °C with Rodent decloaker buffer (Biocare Medical). After blocking non-specific sites with 1% bovine serum albumin, sections were incubated with rabbit anti-von Willebrand factor (vWF, DakoCytomation) followed by Alexa Fluor 546 donkey anti-rabbit secondary antibody (Molecular Probes), or Cy3-conjugated alpha-smooth muscle actin (α-SMA, Sigma Aldrich). Cell nuclei were labelled with 4′-6-diamidino-2-phenylindole, and structures with fluorescein wheat germ agglutinin (Vector Laboratories). Fluorescence was examined using an inverted confocal laser-scanning microscope (Leica TCS SP8, Leica microsystems).

2.6. Statistical analysis

Data were expressed as means ± standard deviations. The normality of data distribution was verified by means of Shapiro–Wilk test. Unpaired t-test or Mann–Whitney test was performed to compare two

groups in case of normal and non-normal distribution, respectively; ANOVA or Kruskal–Wallis test, followed by Dunn's post-hoc test, was used for multiple comparisons. Finally, correlations between variables were checked by means of Pearson or Spearman coefficients. A p-value < 0.05 was considered as statistically significant.

3. Results

3.1. Morphological and dimensional analysis

Macroscopically, both 3L Silkothane® and 1L SF grafts (figures 1(c) and (d)) are white and brittle when dry and become more ductile and pliable when hydrated, with a tendency to regain the original shape after manual deformation. In such state, 1L SF grafts are still less deformable and more transparent than 3L Silkothane® group. From wet to dry conditions, they shrink of about $9 \pm 1\%$ in case of 3L Silkothane® and $14 \pm 2\%$ for 1L SF ($p < 0.01$), their thickness mean values are 0.14 ± 0.02 and 0.09 ± 0.01 mm ($p < 0.001$) while their diameters are 1.36 ± 0.08 and 1.41 ± 0.11 mm, respectively. 3L Silkothane® grafts are slightly denser than 1L SF ones (0.69 ± 0.43 and 0.49 ± 0.21 g cm^{-3}) despite a non-negligible intra-class variability and no statistical difference among the two groups.

The morphological observations via SEM highlight that the diameter of SF fibres of 3L Silkothane® and 1L SF grafts are slightly different in the inner layer (0.70 ± 0.19 vs 0.65 ± 0.26 µm, $p < 0.05$, table 2), while the discrepancy in the other layer is more pronounced (0.51 ± 0.14 vs 0.38 ± 0.12 µm, $p < 0.001$, table 2). Frequency distributions of fibres' diameter are all positively skewed (figures 2(e)–(h)). In all layers SF fibres are also randomly arranged, with no preferential orientation in a specific direction (figures 2(i)–(l)). Focusing on the cross-sections (figures 1(i) and (j)), in 3L Silkothane® grafts the multi-layered structure is not detectable, despite being manufactured in subsequent phases (higher magnification available as supplementary material). This likely testifies a good cohesion between the overlapped electrospun layers.

Averaged thicknesses of AA and VC are significantly different, being 0.14 ± 0.03 mm and 0.02 ± 0.00 mm, respectively ($p < 0.05$). Similarly, a different *in vivo* tensioning is observed between arteries and veins ($56 \pm 8\%$ vs $148 \pm 32\%$, $p < 0.001$). In terms of thickness, VC significantly differs from 3L Silkothane® and 1L SF grafts ($p < 0.001$), as well, while grafts thickness is comparable to the one of AA.

All the results are recapitulated in table 2.

3.2. Mechanical and physical characterization

3.2.1. Radial compliance

3L Silkothane® and 1L SF electrospun grafts share comparable radial compliances in all the considered pressure ranges (50–90 mmHg, 80–120 mmHg and 110–150 mmHg) without significant differences between the two groups (figure 5(a)). When comparing hypo- (50–90 mmHg) and normotension (80–120 mmHg) conditions, hybrid grafts are generally more compliant than pure SF ones, having compliances of 1.88 ± 1.01 and $1.85 \pm 1.02\%$ 10^{-2} mmHg^{-1} against 1.35 ± 0.51 and $1.68 \pm 0.45\%$ 10^{-2} mmHg^{-1}, respectively. Conversely, in case of hypertension conditions (110–150 mmHg) they are less prone to dimensional variations in response to a pressure gradient, as their compliance is $1.37 \pm 0.86\%$ 10^{-2} mmHg^{-1} against $1.53 \pm 0.36\%$ 10^{-2} mmHg^{-1} of 1L SF. Radial compliance of 3L Silkothane® grafts decreases from hypo- to hypertension, while a similar trend is not detected in case of 1L SF. Rats' AA shows higher radial compliance values than electrospun grafts, being of 37 ± 5.46, 17.76 ± 3.08 and $8.53 \pm 1.57\%$ 10^{-2} mmHg^{-1} in the ranges of 50–90, 80–120 and 110–150 mmHg, respectively ($p < 0.01$–0.001, figure 5(b)). These radial compliances, which decrease with increasing pressure, are significantly different among them ($p < 0.001$). VC was tested in lower pressure ranges (10–20, 20–30 and 30–40 mmHg), better representing venous physiological conditions.

There, radial compliances are 116.72 ± 65.67, 53.63 ± 31.72 and $33.78 \pm 17.72\%$ 10^{-2} mmHg^{-1} with significant difference between the low-pressure regime and the other two groups ($p < 0.05$) (figure 5(b)). As analysed pressure ranges of VC are different, no comparisons can be made with AA or electrospun grafts. Diameter distensibility of AA rat arteries is equal to 1.00 ± 0.13 10^{-2} mmHg^{-1} in the 0–100 mmHg pressure range.

3.2.2. Viscoelasticity

Both in case of 3L Silkothane® and 1L SF grafts, the diameter at 100 mmHg increase between the first and the 15th cycle, confirming the viscoelastic behaviour of the devices. On average, 3L Silkothane® grafts deform more than 1L SF ones ($0.76 \pm 0.53\%$ vs $0.52 \pm 0.41\%$, figure 4(a)), despite a non-statistical difference. As regards the hysteresis curves, in both cases the included area decreases from the first to the last cycle (figure 5(c)).

3.2.3. Water permeability

Water permeability significantly differs between 3L Silkothane® and 1L SF grafts, being 0.43 ± 0.33 and 1.31 ± 1.12 ml cm^{-2} min^{-1}, respectively ($p < 0.05$, table 2).

3.3. Preliminary implantation tests

All the rats survived the surgery without complications, such as internal haemorrhaging or paraplegia due to the bloodstream deviation in case of peripheral shunt. Operators evaluated that 3L Silkothane® grafts structure and characteristics were optimal to perform

Table 2. Morphological, dimensional and physical characteristics of electrospun grafts (3L Silkothane® and 1L SF) and rat native vessels: abdominal aorta (AA) and vena cava (VC). th: wall thickness, D: internal diameter, ρ: density, K: permeability, $\Phi_{SF\text{-}fibres}$: silk fibroin fibres diameter. Results are expressed as mean ± standard deviation.

	3L Silkothane®	1L SF	AA	VC
th (mm)	0.14 ± 0.02	0.10 ± 0.04	0.14 ± 0.03	0.02 ± 0.00
D (mm)	1.36 ± 0.08	1.41 ± 0.11	—	—
ρ (g cm^{-3})	0.69 ± 0.43	0.49 ± 0.21	—	—
Deformation$_{wet\text{-}dry}$ (%)	9 ± 1	14 ± 2	—	—
In vivo tensioning (%)	—	—	56 ± 8	148 ± 32
K (ml cm^{-2} min^{-1})	0.43 ± 0.33	1.31 ± 1.12	—	—
$\Phi_{SF\text{-}fibres\ IN}$ (μm)	0.70 ± 0.19	0.65 ± 0.26	—	—
$\Phi_{SF\text{-}fibres\ OUT}$ (μm)	0.51 ± 0.14	0.38 ± 0.12	—	—

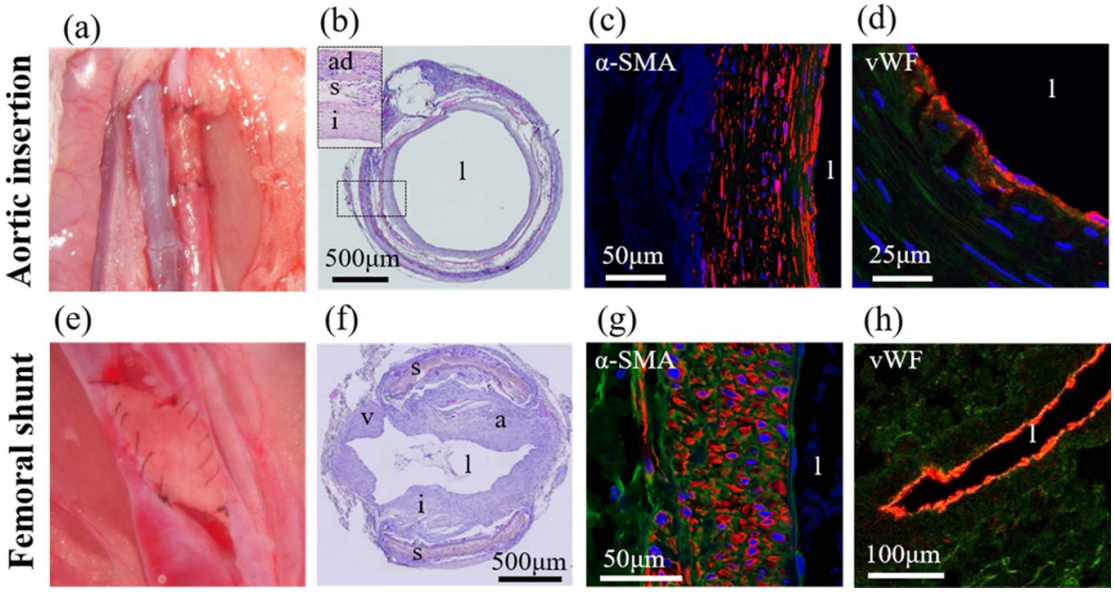

Figure 5. Evaluation of 3L Silkothane® grafts during preliminary implantation tests: (a) aortic insertion right after the surgery; (b) histology of the aortic insertion after animal's sacrifice (three months after the surgery); representative immunofluorescence staining of α-SMA ((c), red) and vWF ((d), red) of the aortic insertion; (e) femoral shunt right after the surgery; (f) histology of the femoral shunt after animal's sacrifice (three months after surgery); representative immunofluorescence staining of α-SMA ((g), red) and vWF ((h), red) of the femoral shunt. Ad: adventitia, s: 3L Silkothane®, i: intima, v: vein, a: artery, l: lumen.

aortic insertions (figure 4(a)), providing an adequate mechanical support for high pressure of this anatomic district. On the contrary, they were less manageable when used to create the femoral shunt (figure 4(e)). Despite different size between native vessels and the graft, all the implants were successful.

Ten rats out of ten and six out of seven who received the aortic insertion and the femoral shunt, respectively, survived with blood flow inside the graft until the end-point (three months). Only in one femoral shunt, Echo-Doppler evaluation highlighted the absence of blood flow 14 days after surgery. Once harvested, histologic analysis was performed to understand the geometry and the cellular composition of both grafts. Sections of aortic insertion (figure 4(b)) showed an outer layer of adventitia, a middle layer with 3L Silkothane® graft, the media with smooth muscle cells (SMCs) (figure 4(c)), and an inner one of intima which includes vWF-positive endothelial cells (figure 4(d)). No abnormal cell proliferation of the intimal layer and consequent stenosis of the vessels was observed in any of the rats that underwent surgery. As for femoral shunts, different sections were obtained at different depths to examine the tissue architecture. As shown in figure 4(f), the artery and vein were connected to the newly generated tissue to form a single lumen surrounded by 3L Silkothane® graft, a medial layers mostly composed of α-SMA-positive cells (figure 4(g)) and finally an endothelial cell layer expressing vWF (figure 4(h)). A slight thickening of the inner intima layer was observed, without however observing vessel occlusion.

4. Discussion

The present study focused on the scaling of Silkothane® medium size vascular grafts (Ø = 6 mm) down to the very small-calibre (Ø = 1.5 mm), fabricating and characterizing three-layered tubular samples (3L Silkothane®), in which a Silkothane® core is enclosed between an inner and an outer layer

of SF, and a control group of pure SF grafts (1L SF). A rodent model was adopted to verify the surgical usability of 3L Silkothane® grafts in arterial and in an arterio-venous configuration. Rats' AAs and VCs were mechanically tested similarly to grafts.

The manufacturing of small-calibre grafts was successfully achieved thanks to an adjustment of the electrospinning protocol developed by van Uden *et al* [35] for medium-calibre grafts. The optimization phase consisted in iteratively acting on process parameters (ΔV, Q, ω, d, table 2), referring to the review study of Catto *et al* [9] to achieve a macroscopic morphologic repeatability of the samples. Considering microstructure, the electrospinning technique generated tubular scaffolds composed of nano-fibrous meshes that mimic the extracellular matrix (ECM) morphology of biological tissues [47].

Concerning average diameter, SEM analysis highlighted differences between SF fibres of both the inner and the outer layers of 3L Silkothane® and 1L SF grafts. Within the same group, the inner layer regularly shows a higher average diameter with respect to the outer one (table 2), as fibres probably pack themselves on the collector after the impact. Conversely, no differences were observed regarding their orientation, as they were randomly arranged in all layers. The good cohesion between subsequent layers of 3L Silkothane® grafts observed on their cross sections (figure 1(i)) is encouraging, since it may avoid fluid infiltration and stagnation between layers that could trigger thrombotic phenomena when implanted *in vivo*. At the sight, small-calibre grafts look similar to medium-calibre three-layered samples [35], with analogous behaviour when dry and when hydrated. The longitudinal shrinkage from dry to wet conditions is more evident in case of 1L SF than 3L Silkothane® grafts ($p < 0.01$, table 2), which testifies that SF is more prone to shrinking than PU. This phenomenon does not result in a denser structure; in fact, average dry density is higher in case of 3L Silkothane® than 1L SF grafts (table 2) with no correlation between these parameters. Moreover, density's standard deviations suggest a non-negligible intra-class variability, which anyway results in no statistical difference among the two groups. Conversely, differences were found comparing grafts thicknesses ($p < 0.001$, table 2), even though both 1L and 3L groups are comparable to rats' AA; on the contrary, VC thickness is significantly lower than arteries ($p < 0.05$) and grafts ($p < 0.001$). The observed discrepancies in terms of native vessel walls' thickness and tissue architecture (figures 1(k) and (l)) match with different *in vivo* tensioning values. Indeed AA, which are thicker and provided with musculature [48], are less stretched than VC ($p < 0.001$, table 2).

Electrospun grafts were mechanically tested in terms of radial compliance, viscoelasticity and water permeability in an on-purpose designed custom experimental set up (figure 3(a)), with the aim of investigating possible differences induced by the presence of the Silkothane® core within the graft. 3L Silkothane® grafts are less permeable to water than 1L SF grafts (table 2), but the non-negligible standard deviations highlight a significant intra-class variability. Anyway, the obtained results are comparable with the ones of other vascular prostheses developed and implanted in animal models [49, 50], and are in accordance with the suggested values for implantability (<50 ml cm^{-2} min^{-1}, [49]), although it is difficult to compare grafts of different composition and differently manufactured. In both families of grafts, the diameter at 100 mmHg was monitored over 15 stimulation cycles and a percentage increase between the first and the last one was recorded in both 3L Silkothane and 1L SF grafts, being of 0.76 $\pm$ 0.53% and 0.52 $\pm$ 0.41%, respectively (figure 5(c)). Such results confirm the presence of a residual deformation, which is indicative of a viscoelastic behaviour. The same conclusion could be drawn by observing the hysteresis loops (figure 5(d)), whose areas decrease from the first to the 15th cycle. Even though the presence of PU in the core of 3L Silkothane® grafts was expected to remarkably improve elasticity and deformability, their radial compliance was found to barely exceed 1L SF only in case of hypo- (1.88 $\pm$ 1.01 against 1.35 $\pm$ 0.51% 10^{-2} $mmHg^{-1}$) and normotension (1.85 $\pm$ 1.02 against 1.68 $\pm$ 0.45% 10^{-2} $mmHg^{-1}$), while it is lower in hypertension conditions (1.37 $\pm$ 0.86 against 1.53 $\pm$ 0.36% 10^{-2} $mmHg^{-1}$, figure 5(a)). Such similarity between the compliances of the two groups could be ascribed to the peculiar structure of 3L samples, whereas the pure-SF coating constrains the dimensional expansion of the Silkothane® core. Differently from medium-calibre vascular grafts [35], where the reduced thickness/radius ratio allowed to amplify the influence of PU on Silkothane® graft's global behaviour, very small calibres tend to hide this potentiality. Moreover, the matrices of SF fibres in the inner and the outer layers of both groups appeared dense and tight when observed at SEM (figures 2(a)–(d)), likely justifying the reduced deformability of the grafts. The attained results in terms of radial compliance can be compared with literature data, keeping in mind that the comparisons between results reported in different studies require a careful analysis, as the adopted setups, protocols, and applied formulas are not homogeneous. For example, Wise *et al* [21] developed a device ($Ø_{ext}$ = 3.5 mm) composed of recombinant human tropoelastin and polycaprolactone (PCL), measuring a radial compliance of 0.006% 10^{-2} $mmHg^{-1}$, likely ascribable to the rigid behaviour of PCL. Khodadoust *et al* [51] evaluated three grafts ($Ø_{in}$ = 5 mm) of different composition: pure-PU, PET, and hybrid PU/PET. They observed that compliance of the PU/PET scaffold (4.47 $\pm$ 0.18% 10^{-2} $mmHg^{-1}$) is higher

than that of PET ($1.75 \pm 0.13\%$ 10^{-2} $mmHg^{-1}$) but lower than the one composed of pure PU ($14.10 \pm 1.00\%$ 10^{-2} $mmHg^{-1}$), confirming that, as initially hypothesized, the presence of PU enhances the deformability of a device. On those calibres, and in absence of rigid inner and outer layers, such potentiality of PU is considerable. de Valence *et al* [52] used PCL to electrospin a vascular graft (Øin = 2 mm) with an *in vivo* compliance of $7.8 \pm 0.9\%$ 10^{-2} $mmHg^{-1}$ in line with our measurements on biohybrid grafts, while Gupta *et al* [53] processed silk fibroin ($Ø_{in} = 1$ mm) obtaining a compliance of 1%–1.5% 10^{-2} $mmHg^{-1}$, which is also comparable with our SF grafts.

Our very small calibre grafts in 3L Silkothane® and 1L SF were developed and optimized for their use and evaluation for arterial and arteriovenous interposition in rodent model. Being the rodent model one of the most used animal models in research and pre-clinical assessment of implantable devices such as patches, grafts and scaffolds in general, we performed a systematic characterization of rat's main native vessels, selecting AA and VC as representative vessels for *in vivo* implantations. Indeed, to our knowledge there are no specific data about radial compliance values of aortic arteries and venae of rats, while vessels related to other bigger animal models, such as ovine or pig are better characterized in terms of compliance/distensibility and mechanical properties, being preferred and widely used in preclinical assessment [54]. Not surprisingly, compliance values obtained from our experiments showed that rats' AA is more deformable than electrospun grafts ($p < 0.01$–0.001) in all the considered pressure ranges (50–90, 80–120, and 110–150 mmHg), showing a decreasing radial compliance conversely to pressure (figure 5(b)). The obtained *ex vivo* compliance measurements are comparable with literature *in vivo* estimations, considering the same anatomical district in the 80–120 mmHg pressure range (17.76 ± 3.08 against $21.0 \pm 2.8\%$ 10^{-2} $mmHg^{-1}$ [52]). In addition, distensibility values calculated for rat AAs (1.00 ± 0.13 10^{-2} $mmHg^{-1}$) are consistent and slightly higher than those measured from rat's carotid arteries (0.77 ± 0.16 10^{-2} $mmHg^{-1}$) [55]. This difference is expected, being aortas highly compliant vessels due to their greater elastin content [56]. Comparing our data on rat arterial compliance with data obtained in humans in the 80–120 mmHg pressure range [57] we observe that rat arteries are about three times more compliant than human arteries, which are in the range 4.4%–7.9% 10^{-2} $mmHg^{-1}$. This behaviour is in line with literature data showing that, considering the same anatomical district, vascular compliance decreases with increasing animal size [55]. As concerns the venous compartment, VC compliance values cannot be directly compared to those of AA nor to 3L Silkothane® and 1L SF electrospun grafts, since analysed pressure ranges are different (10–20, 20–30, 30–40 mmHg vs 50–90, 80–120, 110–150 mmHg). In fact, VC was evaluated among lower pressure ranges that better mimic the *in vivo* conditions [43] (figure 5(b)). Similarly, no comparisons with literature data are possible for the lack of data on distensibility of rodent venous vessels.

Concerning the potential of small-calibre 3L Silkothane® grafts to be implanted as arterial and arteriovenous interpositions in rats, our study preliminarily confirmed that, despite the mismatch in diameter and thickness between grafts and native vessels, 3L Silkothane® grafts can be easily implanted, they exhibit excellent pliability and good suturability especially when used as aortic insertions (figure 4(a))—as previously observed for pure fibroin grafts in [45, 46]. Indeed, as evidenced by echo-Doppler measurements and by morphological evaluations, in all cases—except one—3L Silkothane® grafts remained patent for three months, both when implanted as aortic insertions and as arteriovenous shunts. Not surprisingly, the application in the arteriovenous configuration elicited a more aggressive host reaction, in particular at the venous anastomosis. Here, the exacerbated mismatch in compliance between the graft and the downstream venous vessel (average values of 1.88% 10^{-2} $mmHg^{-1}$ vs 33.78% 10^{-2} $mmHg^{-1}$ in the pressure ranges 30–40 and 50–90 mmHg, respectively) is thought to generate abnormal hemodynamic conditions, which in turn induce extensive formation of endoluminal matrix of fibrotic origin, as shown by the histological analysis. Interestingly, in six out of seven cases, the grafts were patent at explant while lumen restriction resulted in the graft's occlusion only in one case at three months. These results outperform the ones typically found with fully synthetic materials, as demonstrated by several research groups that used them as control. For example, Lovett *et al* [46] observed occlusion in PTFE grafts ($D = 2$ mm, aortic insertion in a rodent model) 24 h after surgery, while Mugnai *et al* [58] in two rats over six that received ePTFE grafts ($D = 2$ mm) as infrarenal aortic replacements. In light of that, the success rate of the performed implants of 3L Silkothane® grafts is considered to be satisfactory and comparable in terms of patency, integration with the anatomical site and remodelling, with autologous decellularized heterologous grafts, as calcification was absent, too. The success rate of the performed implants is satisfactory and comparable in terms of patency, integration with the anatomical site and remodelling with autologous and decellularized heterologous grafts [59].

5. Conclusion

In this study, we successfully demonstrated the possibility to manufacture small-calibre three-layered Silkothane® grafts via electrospinning, obtaining a device with shape and consistency similar to

the medium-calibre one. Despite the unexpressed influence of Silkothane® on the mechanical behaviour of these grafts, specifically comparing their radial compliance with the one of pure SF ones, we were able to develop a solid protocol for the *ex vivo* characterization, which enabled the study of biological vessels, as well. Furthermore, to the best of our knowledge, the measured compliance values of rats' vessels are rarely reported in literature and represent relevant and useful biological data in the scientific scenario, as rodents are a widely adopted animal model. These results will be useful in future studies aimed at the understanding of the interaction between the device and the implant site. Preliminary *in vivo* evaluations confirmed the suitability of Silkothane® grafts for small-calibre applications, with promising outputs in rodent model especially as regards aortic insertion. Further studies will allow the assessment of the performances on longer timepoints, analysing the potentialities in terms of degradability and tissue formation.

Data availability statement

The data that support the findings of this study are available upon reasonable request from the authors.

Acknowledgments

This paper is part of the dissemination activities of Silkelastograft project. This research was funded by the Fondazione Cariplo and Regione Lombardia(Project Number: 2018-1777).

ORCID iDs

Elia Pederzani https://orcid.org/0000-0002-6825-8070
Sonia Fiori https://orcid.org/0000-0002-6291-6415
Matteo Tironi https://orcid.org/0000-0002-1940-5273
Paola Rizzo https://orcid.org/0000-0001-9160-8000
Fabio Sangalli https://orcid.org/0000-0001-5912-0312
Marina Figliuzzi https://orcid.org/0000-0002-3239-2585
Stefania Adele Riboldi https://orcid.org/0000-0003-4025-6249
Monica Soncini https://orcid.org/0000-0001-8607-7196

References

[1] World Health Organization 2021 *World Health Statistics 2021: Monitoring Health for the SDGs, Sustainable Development Goals* (Geneva: World Health Organization)
[2] Alexander J H, Smith P K and Jarcho J A 2016 Coronary-artery bypass grafting *New Engl. J. Med.* **374** 1954–64
[3] Brown R S 2020 Barriers to optimal vascular access for hemodialysis *Semin. Dial.* **33** 457–63
[4] Bordenave L, Menu P and Baquey C 2008 Developments towards tissue- arterial substitutes *Tissue Eng.* **5** 337–47
[5] Abbott W M, Green R M, Matsumoto T, Wheeler J R, Miller N, Veith F J, Suggs W D, Hollier L, Money S and Garrett H E 1997 Prosthetic above-knee femoropopliteal bypass grafting: results of a multicenter randomized prospective trial *J. Vasc. Surg.* **25** 19–28
[6] Xue L and Greisler H P 2003 Biomaterials in the development and future of vascular grafts *J. Vasc. Surg.* **37** 472–80
[7] Bhattacharya V, McSweeney P A, Shi Q, Bruno B, Ishida A, Nash R, Storb R F, Sauvage L R, Hammond W P and Wu M H-D 2000 Enhanced endothelialization and microvessel formation in polyester grafts seeded with CD34+ bone marrow cells *Blood* **95** 581–5
[8] Kannan R Y, Salacinski H J, Butler P E, Hamilton G and Seifalian A M 2005 Current status of prosthetic bypass grafts: a review *J. Biomed. Mater. Res.* B **74** 570–81
[9] Catto V, Farè S, Freddi G and Tanzi M C 2014 Vascular tissue engineering: recent advances in small diameter blood vessel regeneration *ISRN Vasc. Med.* **2014** 1–27
[10] Rathore A, Cleary M, Naito Y, Rocco K and Breuer C 2012 Development of tissue engineered vascular grafts and application of nanomedicine *Wiley Interdiscip. Rev. Nanomed. Nanobiotechnol.* **4** 257–72
[11] Salacinski H J, Goldner S, Giudiceandrea A, Hamilton G, Seifalian A M, Edwards A and Carson R J 2001 The mechanical behavior of vascular grafts: a review *J. Biomater. Appl.* **15** 241–78
[12] Couet F, Rajan N and Mantovani D 2007 Macromolecular biomaterials for scaffold-based vascular tissue engineering *Macromol. Biosci.* **7** 701–18
[13] Sengupta D, Waldman S D and Li S 2014 From *in vitro* to *in situ* tissue engineering *Ann. Biomed. Eng.* **42** 1537–45
[14] Gong W *et al* 2016 Hybrid small-diameter vascular grafts: anti-expansion effect of electrospun poly ε-caprolactone on heparin-coated decellularized matrices *Biomaterials* **76** 359–70
[15] Fioretta E S, Fledderus J O, Burakowska-Meise E A, Baaijens F P T, Verhaar M C and Bouten C V C 2012 Polymer-based scaffold designs for *in situ* vascular tissue engineering: controlling recruitment and differentiation behavior of endothelial colony forming cells *Macromol. Biosci.* **12** 577–90
[16] Zhang L, Liu X, Li G, Wang P and Yang Y 2019 Tailoring degradation rates of silk fibroin scaffolds for tissue engineering *J. Biomed. Mater. Res.* A **107** 104–13
[17] Zhang H, Zhou L and Zhang W 2014 Control of scaffold degradation in tissue engineering: a review *Tissue Eng.* B **20** 492–502
[18] Lyu L, Schley J, Loy B, Lind D, Hobot C, Sparer R and Untereker D 2007 Kinetics and time-temperature equivalence of polymer degradation *Biomacromolecules* **8** 2301–10
[19] Bockeria L A, Svanidze O, Kim A, Shatalov K, Makarenko V, Cox M and Carrel T 2017 Total cavopulmonary connection with a new bioabsorbable vascular graft: first clinical experience *J. Thorac. Cardiovascular Surg.* **153** 1542–50
[20] Bockeria L, Carrel T, Lemaire A, Makarenko V, Kim A, Shatalov K, Cox M and Svanidze O 2020 Total cavopulmonary connection with a new restorative vascular graft: results at 2 years *J. Thorac. Dis.* **12** 4168–73
[21] Wise S G, Byrom M J, Waterhouse A, Bannon P G, Ng M K C and Weiss A S 2011 A multilayered synthetic human elastin/polycaprolactone hybrid vascular graft with tailored mechanical properties *Acta Biomater.* **7** 295–303
[22] Centola M, Rainer A, Spadaccio C, de Porcellinis S, Genovese J A and Trombetta M 2010 Combining

electrospinning and fused deposition modeling for the fabrication of a hybrid vascular graft *Biofabrication* **2** 014102
[23] Nishita M *et al* 2017 Small-diameter hybrid vascular grafts composed of polycaprolactone and polydioxanone fibers *Sci. Rep.* **7** 1–11
[24] McCarthy C W, Ahrens D C, Joda D, Curtis T E, Bowen P K, Guillory R J, Liu S Q, Zhao F, Frost M C and Goldman J 2015 Fabrication and short-term *in vivo* performance of a natural elastic lamina-polymeric hybrid vascular graft *ACS Appl. Mater. Interfaces* **7** 16202–12
[25] Zhang F, Bambharoliya T, Xie Y, Liu L, Celik H, Wang L, Akkus O and King M W 2021 A hybrid vascular graft harnessing the superior mechanical properties of synthetic fibers and the biological performance of collagen filaments *Mater. Sci. Eng.* C **118** 111418
[26] Jirofti N, Mohebbi-Kalhori D, Samimi A, Hadjizadeh A and Kazemzadeh G-H 2019 Fabrication and characterization of novel compliant small-diameter PET/PU/PCL triad-hybrid vascular graft *Biomed. Mater.* **15** 055004
[27] Shimada K, Higuchi A, Kubo R, Murakami T, Nakazawa Y and Tanaka R 2017 The effect of a silk fibroin/polyurethane blend patch on rat vessels *Organogenesis* **13** 115–24
[28] Chiarini A, Petrini P, Bozzini S, dal Pra I and Armato U 2003 Silk fibroin/poly(carbonate)-urethane as a substrate for cell growth: *in vitro* interactions with human cells *Biomaterials* **24** 789–99
[29] Zhou M, Wang W-C, Liao Y-G, Liu W-Q, Yu M and Ouyang C-X 2014 *In vitro* biocompatibility evaluation of silk-fibroin/polyurethane membrane with cultivation of HUVECs *Front. Mater. Sci.* **8** 63–71
[30] Petrini P, Chiarini A, Bozzini S, dal Pra I, Fare' S and Armato' U 2002 Silk fibroin-polyurethane scaffolds for tissue engineering (https://doi.org/10.1109/MCTE.2002.1174995)
[31] van Uden S, Catto V, Perotto G, Athanassiou A, Redaelli A C L, Greco F G and Riboldi S A 2019 Electrospun fibroin/polyurethane hybrid meshes: manufacturing, characterization, and potentialities as substrates for haemodialysis arteriovenous grafts *J. Biomed. Mater. Res.* B **107** 807–17
[32] Zhang X, Reagan M R and Kaplan D L 2009 Electrospun silk biomaterial scaffolds for regenerative medicine *Adv. Drug Deliv. Rev.* **61** 988–1006
[33] Radakovic D, Reboredo J, Helm M, Weigel T, Schürlein S, Kupczyk E, Leyh R G, Walles H and Hansmann J 2017 A multilayered electrospun graft as vascular access for hemodialysis *PLoS One* **12** e0185916
[34] Rocco K A, Maxfield M W, Best C A, Dean E W and Breuer C K 2014 *In vivo* applications of electrospun tissue-engineered vascular grafts: a review *Tissue Eng.* B **20** 628–40
[35] van Uden S *et al* 2019 A novel hybrid silk-fibroin/polyurethane three-layered vascular graft: towards *in situ* tissue-engineered vascular accesses for haemodialysis *Biomed. Mater.* **14** 025007
[36] Riboldi S A *et al* 2020 A novel hybrid silk fibroin/polyurethane arteriovenous graft for hemodialysis: proof-of-concept animal study in an ovine model *Adv. Healthcare Mater.* **9** 1–11
[37] Catto V, Farè S, Cattaneo I, Figliuzzi M, Alessandrino A, Freddi G, Remuzzi A and Tanzi M C 2015 Small diameter electrospun silk fibroin vascular grafts: mechanical properties, *in vitro* biodegradability, and *in vivo* biocompatibility *Mater. Sci. Eng.* C **54** 101–11
[38] Dörr W and Weber-Frisch M 1997 Shrinking processes in frozen sections *Microsc. Res. Tech.* **599** 598–9
[39] Kotb B S 2001 Comparative study on the effect of some histological techniques on the quantitative morphometric analysis *Egypt. J. Hosp. Med.* **3** 177–89
[40] Johnson R, Ding Y, Nagiah N, Monnet E and Tan W 2019 Coaxially-structured fibres with tailored material properties for vascular graft implant *Mater. Sci. Eng.* C **97** 1–11
[41] Furdella K J, Higuchi S, Behrangzade A, Kim K, Wagner W R and Vande Geest J P 2021 *In-vivo* assessment of a tissue engineered vascular graft computationally optimized for target vessel compliance *Acta Biomater.* **123** 298–311
[42] ISO 7198:2016(E) 2016 *Cardiovascular Implants and Extracorporeal Systems—Vascular Prostheses—Tubular Vascular Grafts and Vascular Patches* (International Organisation for Standardization)
[43] Desch G W and Weizsäcker H W 2007 A model for passive elastic properties of rat vena cava *J. Biomech.* **40** 3130–45
[44] Cops J, Haesen S, de Moor B, Mullens W and Hansen D 2019 Current animal models for the study of congestion in heart failure: an overview *Heart Fail. Rev.* **24** 387–97
[45] Cattaneo I, Figliuzzi M, Azzollini N, Catto V, Farè S, Tanzi M C, Alessandrino A, Freddi G and Remuzzi A 2013 *In vivo* regeneration of elastic lamina on fibroin biodegradable vascular scaffold *Int. J. Artif. Organs* **36** 166–74
[46] Lovett M, Eng G, Kluge J A, Cannizzaro C, Vunjak-Novakovic G and Kaplan D L 2010 Tubular silk scaffolds for small diameter vascular grafts *Organogenesis* **6** 217–24
[47] Cui W, Zhou Y and Chang J 2010 Electrospun nanofibrous materials for tissue engineering and drug delivery *Sci. Technol. Adv. Mater.* **11** 014108
[48] dela Paz N G and D'Amore P A 2009 Arterial versus venous endothelial cells *Cell Tissue Res.* **335** 5–16
[49] Huang F, Sun L and Zheng J 2008 *In vitro* and *in vivo* characterization of a silk fibroin-coated polyester vascular prosthesis *Artif. Organs* **32** 932–41
[50] Aytemiz D, Sakiyama W, Suzuki Y, Nakaizumi N, Tanaka R, Ogawa Y, Takagi Y, Nakazawa Y and Asakura T 2013 Small-diameter silk vascular grafts (3 mm diameter) with a double-raschel knitted silk tube coated with silk fibroin sponge *Adv. Healthcare Mater.* **2** 361–8
[51] Khodadoust M, Mohebbi-Kalhori D and Jirofti N 2018 Fabrication and characterization of electrospun bi-hybrid PU/PET scaffolds for small-diameter vascular grafts applications *Cardiovascular Eng. Technol.* **9** 73–83
[52] de Valence S, Tille J-C, Mugnai D, Mrowczynski W, Gurny R, Möller M and Walpoth B H 2012 Long term performance of polycaprolactone vascular grafts in a rat abdominal aorta replacement model *Biomaterials* **33** 38–47
[53] Gupta P, Lorentz K L, Haskett D G, Cunnane E M, Ramaswamy A K, Weinbaum J S, Vorp D A and Mandal B B 2020 Bioresorbable silk grafts for small diameter vascular tissue engineering applications: *in vitro* and *in vivo* functional analysis *Acta Biomater.* **105** 146–58
[54] Byrom M J, Bannon P G, White G H and Ng M K C 2010 Animal models for the assessment of novel vascular conduits *J. Vasc. Surg.* **52** 176–95
[55] Prim D A, Mohamed M A, Lane B A, Poblete K, Wierzbicki M A, Lessner S M, Shazly T and Eberth J F 2018 Comparative mechanics of diverse mammalian carotid arteries *PLoS One* **13** 1–18
[56] Jiang L, Chen H, Li R, Han X, Chen Z, He L, Yuan C and Zhao X 2015 Associations of arterial distensibility between carotid arteries and abdominal aorta by MR *J. Magn. Reson. Imaging* **41** 1138–42
[57] Jirofti N, Mohebbi-Kalhori D W, Samimi A, Hadjizadeh A and Kazemzadeh G H 2018 Small-diameter vascular graft using co-electrospun of composite PCL/PU nanofibers *Biomed. Mater.* **13** 055014
[58] Mugnai D, Tille J-C, Mrówczyński W, de Valence S, Montet X, Möller M and Walpoth B H 2013 Experimental noninferiority trial of synthetic small-caliber biodegradable versus stable vascular grafts *J. Thorac. Cardiovascular Surg.* **146** 400–7.e1
[59] Bai H, Wang Z, Li M, Sun P, Wang W, Liu W, Wei S, Wang Z, Xing Y and Dardik A 2020 A rat arteriovenous graft model using decellularized vein *Vascular* **28** 664–72